

## Quantum Chaotic Scattering in Atomic Physics: Ericson Fluctuations in Photoionization

Gernot Stania\* and Herbert Walther

*Max-Planck-Institut für Quantenoptik, D-85748 Garching, Germany*

(Received 1 July 2005; published 1 November 2005)

We report the first experimental investigation of quantum chaotic scattering in an atomic system:  $^{85}\text{Rb}$  in strong crossed magnetic and electric fields in an energy regime beyond the ionization threshold, where the classical dynamics is an example of chaotic scattering. We find Ericson fluctuations in the spectra for photo excitation into this regime. This result constitutes the first observation of Ericson fluctuations in atomic and molecular physics. Furthermore, we confirm the prediction that chaotic scattering in the underlying classical dynamics implies Ericson fluctuations.

DOI: [10.1103/PhysRevLett.95.194101](https://doi.org/10.1103/PhysRevLett.95.194101)

PACS numbers: 05.45.Mt, 32.60.+i, 32.80.Fb, 32.30.Jc

The concept of Ericson fluctuations (EF) was developed in connection with investigations in nuclear physics. Meanwhile, however, it is evident that EF are of much greater significance. They are now considered to be a universal rather than a genuinely nuclear phenomenon [1]. Furthermore, they play a fundamental role in quantum chaotic scattering: Blümel and Smilansky proposed that the canonical quantization of a chaotic scattering system will result in a quantum scattering process with an excitation function that exhibits EF [2]. In this Letter we describe the first experimental investigation of quantum chaotic scattering in atomic physics. We report the first observation of EF in atomic and molecular physics and thus substantiate the universality of EF. Furthermore, our results provide long called-for confirmation for the prediction of Blümel and Smilansky.

EF were originally predicted [3] and observed [4,5] in the excitation functions of compound nuclear reactions. These reactions result from coherent excitation of highly excited states of the compound nucleus and their decay into the exit channels. In the energy regime where the average decay width of these states is much larger than their average spacing (“Ericson regime” of strongly overlapping resonances) the excitation functions are dominated by interference effects. For these functions Ericson predicted fluctuations with a Lorentzian autocorrelation. These fluctuations are now known as EF and have been observed in many compound nuclear reactions [5].

EF are considered to be universal by virtue of the fact that Ericson’s results can be expressed in the following general way [see [1] for details]: an excitation function of any wave-scattering process that has a representation by a many-resonance Breit-Wigner formula will exhibit EF in the regime of strongly overlapping resonances if the statistical distribution of resonance widths is strongly peaked around its mean value and if the resonance amplitudes are random numbers. Breit-Wigner representations, in turn, are universal in the sense that they have been proven to be valid for describing various wave-scattering processes spanning the energy range from the microwave regime [6]

to the many-MeV collisions of nuclear physics [3]. The question whether for such a process the resonance parameters are in accordance with Ericson’s statistical assumptions is much more subtle and interesting. From the experimental point of view, a direct answer is impossible because the strong overlapping of resonances and their interference precludes the possibility of extracting any detailed information about the resonance parameters from measured data. EF can therefore be measured only in the sense that the experimental excitation function is consistent with Ericson’s results, i.e., (i) it has a Breit-Wigner representation, (ii) its structures are dominated by strong overlapping of resonances, and (iii) the autocorrelation of its fluctuation is a Lorentzian with a width larger than the energy resolution. It was exactly in this way that nuclear EF were established experimentally [4]. Beyond nuclear physics there have been experimental investigations of excitation functions of microwave billiards [7] and unimolecular reactions [8] that satisfy prerequisites (i) and (ii). However, a Lorentzian autocorrelation of the fluctuation could not be observed.

It should be noted that Ericson’s results are consistent with random matrix models [9,10]. Against this background, the well-investigated universal conductance fluctuations in the coherent electron transport through mesoscopic samples are analogous to EF [11].

In quantum chaos, Main and Wunner numerically confirmed the connection between chaotic classical scattering and EF for hydrogen in crossed magnetic and electric fields [12]. As opposed to microwave billiards, which are limited to the investigation of two-dimensional quantum chaos [7], alkali atoms in crossed fields can be tuned to a fully chaotic three-dimensional dynamics via experimentally accessible parameters (external fields, energy).

We investigate rubidium ( $^{85}\text{Rb}$ ) in crossed fields. The experiments are performed in a  $^4\text{He}$ -bath cryostat at  $\sim 10^{-8}$  mbar. Rb from an oven is used to form a highly collimated atomic beam. The atoms in the beam pass through a region where they are subjected to the simultaneous influence of a static magnetic induction and an

electric field. Figure 1 depicts the field region schematically: an electromagnet consisting of a pair of superconduction coils in Helmholtz configuration and equipped with a superconducting switch generates a highly stable static magnetic induction. The magnet coils surround a cylinder that contains a plate capacitor for generating the electric field (inner and outer electrodes) and various additional electrodes that serve to detect excited atoms. In the region where the magnetic induction is highly homogeneous and collinear with the atomic beam, the plate capacitor generates an electric field perpendicular to the magnetic induction (crossed fields). Here, two counterpropagating laser beams are focused onto the atomic beam. Their direction is perpendicular to the magnetic induction as well as to the electric field.

In our measurements the magnetic induction is in the range 1–2 T, and the electric field is 22.41(6) kV/m. We investigate the photo excitation to the energy interval  $[-57.08 \text{ cm}^{-1}; -55.92 \text{ cm}^{-1}]$  for different values of the magnetic induction [the zero point of the energy scale is the field-free ionization threshold of  $^{85}\text{Rb}$  [13]]. The energy interval is in the Rydberg regime ( $n \sim 44$ ) and significantly above the Stark-saddle energy ( $-91.4 \text{ cm}^{-1}$ ) corresponding to the electric field. To investigate the photo excitation of a pure internal state of the atom we use a two-step excitation scheme. Both stages are driven with linearly polarized light from frequency-stabilized tunable single-mode cw lasers. In the first step a diode laser in Littrow configuration at  $\sim 780 \text{ nm}$  is tuned into resonance with the (Zeeman-shifted) hyperfine transition between  $5s_{1/2}, f = 3, m_f = -3$  and  $5p_{3/2}, f = 4, m_f = -4$  (intermediate state) (the Stark effect of these states is negligible). A ring-dye laser at  $\sim 480 \text{ nm}$  provides the light for the second step, which makes the Rydberg regime accessible from the intermediate state.

Rydberg atoms are detected by ionization and subsequent electron detection. The ionization takes place in the electrode setup in Fig. 1. The principles of its operation are explained in [14]. In short, this setup works simultaneously

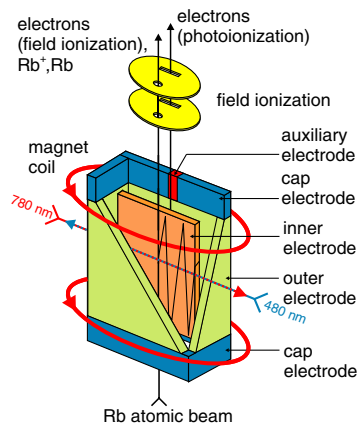


FIG. 1 (color online). Electrode setup.

in the two regimes of slow and fast ionization, these being defined by whether the excited electron moves away from the atomic core slowly or quickly in relation to the time it takes the atom to traverse the space between the excitation area and the upper cap electrode. In the case of slow ionization, the Rydberg atoms are field ionized. Whereas for fast ionization, electrons are guided by the  $\mathbf{E} \times \mathbf{B}$  drift, the cap electrodes confine their motion along the direction of the magnetic induction until the auxiliary electrode extracts them from the “trap” (zigzag line in Fig. 1, photo-ionization signal). After a defocussing stage the electrons hit a position-sensitive detector. The position information confirms that we are entirely in the photo-ionization regime; i.e., we have the process  $h\nu + ^{85}\text{Rb} \rightarrow ^{85}\text{Rb}^* \rightarrow ^{85}\text{Rb}^+ + e^-$ .

At a given photon energy  $h\nu$  the photo-absorption cross section is related to the power  $P$  of the second excitation stage and the number of excited atoms  $N$  detected during a time  $\tau$  by  $\sigma(h\nu) \propto h\nu \langle N \rangle / (P\tau)$  ( $\langle \cdot \rangle$  denotes the expectation value). In this way we measure a quantity that is proportional to the photo-absorption cross section. Making measurements for a densely spaced set of values from the investigated energy interval constitutes measurement of the excitation function. In the following we use the conventional term “spectrum” for “excitation function.”

We stress the fact that the geometry of the experiment and the use of a two-step excitation scheme ensure that the recorded photo-absorption cross sections are to a very good approximation those of a rubidium atom *at rest* prepared in a pure state and subjected to the external fields in the laboratory frame of reference. Applying the general theory of photo absorption to atomic beams not only provides a unified explanation of these features but also leads to the Breit-Wigner representation of the excitation functions. We just state that for each atomic velocity component the apparatus measures the photo-absorption cross section of an atom at rest but subjected to the external fields (static fields and laser light) as referred to the frame moving with the atom. Our geometry minimizes the deviations that are caused by referring the fields to the moving and not to the laboratory frame (mainly motional Stark effect and Doppler effect), while the first step of the excitation scheme prepares a pure internal state. Estimating the residual influence of the velocity distribution of the atomic beam yields a value on the 10 MHz scale. Finally, the Breit-Wigner representation follows from the formula of Rescigno-McKoy for photo absorption [15] by analytic continuation and pole expansion or complex rotation techniques [12]. Fine and hyperfine structures can be taken into account.

The diode-laser frequency is stabilized to a hermetically sealed temperature- and length-stabilized confocal Fabry-Perot interferometer (FPI) and tuned into resonance with the hyperfine transition by maximizing the photo-ionization signal.

The dye-laser frequency is stabilized to a reference FPI. To record a spectrum, we start by stabilizing both lasers to the desired frequencies and measuring these frequencies with a two beam scanning Michelson interferometer. Then the following step is repeated a few thousand times: measurement of dye-laser power, measurement of dye-laser transmission through the length-stabilized FPI, turn-on of electron detection, counting of excited atoms during a fixed detection time  $\tau$ , turn-off of electron detection, scanning of dye laser to an approximately 10 MHz higher frequency, wait cycle for frequency stabilization. The absolute frequency value at the start together with the transmission data of the length-stabilized FPI determines the absolute photon energy.

Our Michelson interferometer is calibrated before and after the recording of a spectrum with the diode laser stabilized to a Lamb dip of a  $\mu$ -metal-shielded saturation spectroscopy of the Rb  $D2$  line [The absolute frequencies of these dips are known with high precision [16]]. Using the diode laser itself for calibration dramatically reduces systematic errors in measurements of diode-laser frequencies to approximately 5 MHz, i.e., to a relative error of  $\sim 10^{-8}$ . The corresponding statistical errors are even smaller. As for the measurement of the frequency of the dye laser, an upper bound for the systematic errors is 200 MHz (mainly due to alignment and to temperature and pressure dependence of the dispersion relation for air). Such an error just causes an overall shift of the frequency scale for the corresponding spectrum.

For each spectrum, the actual strength of the magnetic induction is obtained directly from measurement of the diode-laser frequency after it has been tuned into resonance with the desired hyperfine transition: subtracting the field-free transition frequency yields the Zeeman shift  $\Delta E = -\mu_B B$ , where  $\mu_B$  is Bohr's magneton. This determines the magnetic induction with a relative error of  $\leq 5 \times 10^{-4}$ . The strength of the electric field is obtained by calibrating the plate capacitor. This is done by extracting the stray field and the plate distance from a comparison of experimental and numerical Stark maps in the vicinity of avoided crossings. The voltage across the plates then determines the electric field with a relative error of  $2.5 \times 10^{-3}$ . A temporal change of stray fields could not be observed.

Our spectra were recorded with the polarization of the dye laser in the direction of the magnetic induction. To eliminate the factor of proportionality we normalize each spectrum with respect to its average value  $\bar{\sigma}$  over a 30 GHz interval  $I$  starting at  $-57.08 \text{ cm}^{-1}$ . The result at 2.0045(8) T is depicted in Fig. 2(a). The spectrum has a pronounced fluctuation. Figure 2(b) is a magnification of a 6 GHz section together with the corresponding part of an independent second measurement for the same experimental parameters [the magnetic induction for the latter was measured to be 2.0047(8) T]. Apart from a small overall shift, the two measurements coincide. This demonstrates

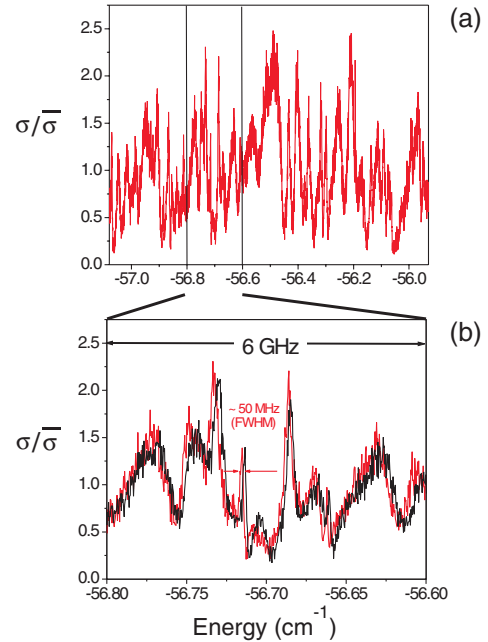


FIG. 2 (color). Measured spectrum.

the high reproducibility of our results. In addition, the section shows a reproducibly resolved narrow peak of  $\sim 50$  MHz FWHM. Since nothing is known about the natural width of structures in crossed fields, this value is a strict upper bound for the structure resolution (experimental linewidth) in crossed fields. A lower bound of 20 MHz FWHM is obtained from field-free spectroscopy of high-lying Rydberg states. The experimental broadening is mainly due to the natural linewidth and saturation broadening in the first excitation stage, while transition time broadening and residual Doppler effect can also be expected to contribute on the MHz scale. Narrow peaks in crossed fields turn out to be very rare. From the figures it follows that the excitation functions are dominated by broader non-Lorentzian structures which have to be interpreted as the result of the overlapping of resonances in the Ericson regime. A rough estimate of the average spacing of resonances is that of field-free hydrogen states in the subspace that is singled out by the selection rules for photo excitation in crossed fields. Even if fine and hyperfine structures are neglected, we arrive at a value of  $\sim 80$  MHz corresponding to several hundreds of overlapping resonances in Fig. 2(a). The true value for the average spacing might be significantly smaller. In any case we are clearly in the Ericson regime. To prove that we really see EF, we compute the autocorrelation of the fluctuation  $\delta\sigma = \sigma - \bar{\sigma}$ :

$$C(\varepsilon) = \frac{1}{\bar{\sigma}^2 |I|} \int_I \delta\sigma(E + \varepsilon) \delta\sigma(E) dE. \quad (1)$$

Here  $I$  is the same interval used to determine  $\bar{\sigma}$ . We compute  $\bar{\sigma}$  and the autocorrelation (1) directly by inter-

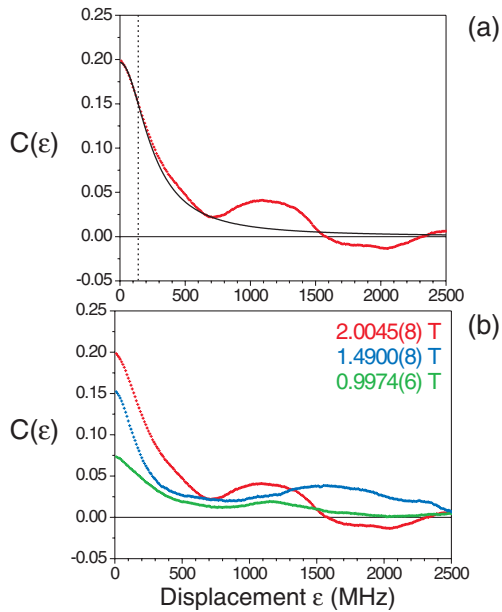


FIG. 3 (color). Ericson fluctuations at different magnetic inductions.

preparing the experimental data as a step function (integrations reduce to finite sums). For the spectrum in Fig. 2(a), the result together with a Lorentzian fit (no offset, no shift) is displayed in Fig. 3(a) and confirms that we have EF. However, at large values of the displacement there are oscillatory deviations from the Lorentzian. The Lorentzian shown in Fig. 3(a) is therefore fitted to the experimental curve in the section from zero displacement up to the dashed line ( $\varepsilon = 140$  MHz). In this region the correlation coefficient is  $>99.8\%$ . Very good agreement of the Lorentzian and the experimental data extends to a 5 times larger section up to roughly  $\varepsilon = 0.7$  GHz. The width of the Lorentzian ( $\sim 0.5$  GHz FWHM) is large compared to our estimate of the average spacing of resonances and at least 1 order of magnitude larger than our energy resolution. Note that the observed width is *10 orders of magnitude* below typical values from nuclear physics. The rather large amplitude of the Lorentzian indicates that we have a small effective number of reaction channels [3]. The oscillatory feature for larger displacements is present in the numerical predictions for hydrogen [12] as well as in the nuclear measurements [4]. For EF in quantum graphs, they are caused by short periodic orbits of the classical dynamics [17]. Whether an analogous explanation holds in our case remains to be investigated.

The parameters for our spectrum at 2.0045(8) T realize to within 1% values at which classical chaotic scattering was found in hydrogen [12,18]. Since the less regular core potential of rubidium cannot be expected to make the crossed-fields dynamics more regular, it is clear that we

have chaotic scattering for rubidium as well. In a next step we investigate the EF as we decrease the magnetic induction. All other experimental parameters remain the same. Figure 3(b) shows the result for 2.0045(8) T together with those for 1.4900(8) T and 0.9974(6) T. Clearly the EF become less pronounced as the magnetic induction decreases. For hydrogen, the same qualitative result has been obtained numerically and correlated with a loss of chaotic features in the classical dynamics (for vanishing magnetic induction the classical hydrogen atom is integrable) [12].

In summary, we have demonstrated EF in the photo excitation of  $^{85}\text{Rb}$  in crossed fields to energies at which the classical dynamics is an example of chaotic scattering. Furthermore, we have shown that the EF become less pronounced as classical chaos decreases. Thereby, we confirm the important prediction of Blümel and Smilansky. In addition, we provide important evidence for the universality of EF: for the first time, EF are observed in atomic and molecular physics.

\*Electronic address: gns@mpq.mpg.de

- [1] S. Y. Kun, Phys. Rev. A **65**, 034701 (2002).
- [2] R. Blümel and U. Smilansky, Phys. Rev. Lett. **60**, 477 (1988).
- [3] T. Ericson, Phys. Rev. Lett. **5**, 430 (1960); Ann. Phys. (N.Y.) **23**, 390 (1963), and references therein.
- [4] P. von Brentano *et al.*, Phys. Lett. **9**, 48 (1964).
- [5] T. Ericson and T. Mayer-Kuckuk, Annu. Rev. Nucl. Sci. **16**, 183 (1966), and references therein.
- [6] J. Stein, H.-J. Stöckmann, and U. Stoffregen, Phys. Rev. Lett. **75**, 53 (1995).
- [7] H.-J. Stöckmann, *Quantum Chaos: An Introduction* (Cambridge University Press, Cambridge, England, 1999), and references therein.
- [8] S. A. Reid and H. Reisler, J. Chem. Phys. **101**, 5683 (1994).
- [9] T. Agassi, H. A. Weidenmüller, and G. Mantzouranis, Phys. Rep. **22**, 145 (1975).
- [10] Y. V. Fyodorov and Y. Alhassid, Phys. Rev. A **58**, R3375 (1998).
- [11] H. A. Weidenmüller, Nucl. Phys. **A518**, 1 (1990).
- [12] J. Main and G. Wunner, Phys. Rev. Lett. **69**, 586 (1992); J. Phys. B **27**, 2835 (1994).
- [13] C.-J. Lorenzen and K. Niemax, Phys. Scr. **27**, 300 (1983).
- [14] G. Raitzel and H. Walther, Phys. Rev. A **49**, 1646 (1994).
- [15] T. N. Rescigno and V. McKoy, Phys. Rev. A **12**, 522 (1975).
- [16] G. P. Barwood, P. Gill, and W. R. C. Rowley, Appl. Phys. B **53**, 142 (1991).
- [17] T. Kottos and U. Smilansky, Phys. Rev. Lett. **85**, 968 (2000).
- [18] G. Stania, Ph.D. thesis, LMU München, 2005.